IEEE Access
Multidisciplinary ⋮ Rapid Review ⋮ Open Access Journal

Received 15 August 2023, accepted 22 September 2023, date of publication 29 September 2023, date of current version 9 October 2023.

Digital Object Identifier 10.1109/ACCESS.2023.3321028

RESEARCH ARTICLE

Design and Analysis of a Novel Compliant Actuator With Variable Stiffness by Spring Pretension Adjustment

YOULEI ZHAO[1], JUNQIANG LIU[2], LI LI[3], AND YAPENG XU[4,5]

[1]Shandong IoT Association, Jinan 250013, China
[2]Inspur Electronic Information Industry Company Ltd., Jinan 250101, China
[3]Jinan Radio Monitoring Station, Jinan 250001, China
[4]School of Mechanical and Electrical Engineering, Zhengzhou University of Light Industry, Zhengzhou 450002, China
[5]Key Laboratory of High Efficiency and Clean Mechanical Manufacture of Ministry of Education, School of Mechanical Engineering, National Demonstration Center for Experimental Mechanical Engineering Education, Shandong University, Jinan 250061, China

Corresponding author: Yapeng Xu (xuyapeng001@mail.sdu.edu.cn)

This work was supported in part by the Doctoral Research Fund of Zhengzhou University of Light Industry under Grant 2022BSJJZK02.

ABSTRACT Variable stiffness actuators (VSA) are an emerging advanced driving method for robotic joint in physical human-robot interaction scenarios. This paper proposes a VSA based on adjusting the pre-tightening force of the driving ropes by rotating the linear springs to change the angle of its axis relative to the input frame. By adjusting the spring angle within a small relative rotation angle stroke, the angle between the spring axis and the transmission rope can be changed, thereby achieving rapid stiffness adjustment in a large range. The characteristics analysis shows that the proposed VSA has good stiffness adjustment independence. The mechanical design scheme of the VSA is introduced in detail. Simulations based on a proportional derivative (PD) controller demonstrated the effectiveness of the design.

INDEX TERMS Mechanism design, robotic joint, variable spring angle mechanism, variable stiffness actuator.

I. INTRODUCTION

Robots are increasingly integrated into the human environment to enable human-machine interaction. The motivation for the growing interest in these topics can be found in the possibilities of using robots for humans, such as exoskeletons, operating in hazardous environments, or helping the elderly or disabled [1], [2]. In order to improve the safety and reliability of physical interaction between robots and humans, robotic systems with abilities of variable stiffness and intrinsic compliance as humans are investigated [3].

In robotic systems, there are generally two approaches to mimic the compliance of human limb movements: one is to use active compliance control at the control algorithm level, such as impedance control, and the other is to adjust the mechanical stiffness of robot joints [4], [5]. Active compliance control for stiff joint relies on proper sensors, parameter identification, accurate dynamic modeling, robust control, etc. Some successful implementations in robotic systems can be found in KUKA [6]. The introduction of elastic elements into the drive chain of robot joint actuators to form a series elastic actuator (SEA) can easily make the robot system intrinsically flexible [7]. Compared to conventional rigid actuators, the elastic element in a SEA significantly reduces the mechanical impedance of the joint, improves the ability to absorb shock loads and peak power [6], and the passive mechanical energy stored by the deformation of the elastic element can be reused, which helps to save energy during cyclic movements [8]. However, the fly in the ointment is that the mechanical stiffness of a traditional SEA is often constant and un-adjustable, which greatly limits its control bandwidth and application.

The associate editor coordinating the review of this manuscript and approving it for publication was Yangmin Li.

To overcome the above limitations, joints with variable stiffness actuators (VSA) that are able to actively change position and stiffness of the output is one of the promising solutions [9]. Classified in terms of the adjustment independence of the output stiffness and position, VSA includes antagonistic motor setup and independent motor setup [10]. In an antagonistic system, two motors and a set of nonlinear spring mechanisms are used to work antagonistically to adjust stiffness and position, just like human skeletal muscles drive joints [11]. Usually, two motor transmission chains are symmetrically arranged, and when they move in the same direction, the joint output position can be controlled. When they move in reverse or differential direction, the joint output stiffness can be adjusted [12]. The antagonistic VSA belongs to the category of adjusting spring preload to change stiffness [13]. Although it can closely mimic the driving mode of human skeletal muscles, its biggest drawback is severe energy consumption and a small range of stiffness adjustment. In addition, the coupling between the output stiffness and position adjustment of the joint is severe, and the control is complex [14].

There are three methods for achieving stiffness adjustment in the independent motor setup VSAs: (1) by adjusting the spring preload, (2) by changing the transmission ratio between the output and elastic element, (3) by changing the physical properties of an elastic elements.

For example, the DLR team used the differential motion of a pair of roller cam mechanisms and the screw to adjust the preload of the spring group to change its balance position, and developed a VS-joint for application on a humanoid robotic arm [15]. In order to make the joint design more compact, the FSJ (Float Spring Joint) was also designed by DLR, a cam roller spring mechanism was adopted as well [16]. Compared to the VS-joint that uses four compression springs, the FSJ only uses one linear floating spring, which effectively improves the compactness of the joint. In addition, the single-sided cam structure in VS-joint has been optimized into a double-sided oblique symmetric cam structure, which can make the stiffness adjustment process smoother. By changing pretension of a nonlinear spring, Mechanically Adjustable Compliance and Controllable Equilibrium Position Actuator (MACCEPA) Has been studied by many scholars [17], [18]. By designing a rope driven winding mechanism, Z. Li et al. proposed a reconfigurable variable preload flexible robot joint named as JVSR [18].

As a typical method of adjusting stiffness based on variable transmission ratio, the lever principle is widely used in VSA. A lever has three principal points: the pivot [19], the spring attachment point, the force point [20]. An actuator with adjustable stiffness (AwAS) was developed based on the method of moving the spring action point while the force action point and the pivot point are relatively fixed [21]. In order to improve the stiffness adjustment range and the compactness of joints, [22], CompAct-VSA [23], [24], [25], [26], etc. fix the spring and the point of force relatively, only changing the position of the lever pivot, achieving a theoretical stiffness adjustment range from zero to infinity. The softer spring and shorter lever make this type of VSAs more compact with a fast stiffness adjustment speed. In addition, the movement direction of the stiffness adjustment mechanism of this type of VSAs is often approximately perpendicular to the direction of lever deflection, which is beneficial for reducing the stiffness adjustment resistance [27]. Liu Z. et al. recently proposed a new VSA based on a second-order lever mechanism by changing the force point, which has wide stiffness regulation range. By employing a novel symmetric structure design and improving the load capacity of the stiffness regulation module, the proposed actuator also shows well performance in load capacity, stiffness regulation response, and elastic hysteresis, which was applied to a multi degree of freedom humanoid robotic arm [28]. Although the principle of adjusting stiffness with variable transmission ratio is relatively simple and significantly improves the range and speed of stiffness adjustment, there is still significant room for improvement in the compactness, power density, and independence of VSA.

Recently, there has been increasing research on the use of changing the physical characteristics of flexible components to achieve stiffness adjustment. From the perspective of material mechanics theory, the bending stiffness EI/L of a beam with small deflection can be adjusted by changing its geometric or material parameters [29]. Adjusting the effective length L of a leaf spring is the easiest method to achieve variable stiffness. Based on this, L. Liu et al. proposed a mechanical-rotary variable impedance actuator (MeRIA) [30]. S. Yang et al. proposed a 2-DOF actuator with variable stiffness by varying the effective length of the springs, which is uniformly distributed in the variable stiffness unit [31]. Y. Xu et al. proposed two compact VSAs based on S-shaped springs, which enables independent, continuous, fast, large range stiffness adjustment by rotating S-springs to change their effective curved beam length [32], [33]. To achieve faster stiffness adjustment, Tyler Morrison et al. present a novel design concept for a robot arm link with variable stiffness based on a rotating beam link (RBL) mechanism to change the inertia I of some paired reverse RBL [34]. In order to change the elastic modulus E of elastic component materials, functional materials are widely used, such as the shape memory alloy [35], the magnetorheological fluid [36], etc. As an example, a linear digital variable stiffness actuator (LDVSA) with variable stiffness mechanism (VSM) based on specially designed S-springs made from shape memory alloy (SMA) is developed by Y. Xu et al. By controlling the temperature of the SMA S-springs with heating wires for different states switching, the actuator stiffness could be discretely configured online [38]. However, changes in material properties E often require a period of power input, so the slow corresponding speed of stiffness is the biggest flaw.

Despite these existing VSA concepts, there remains room for considerable improvement. In this study, a variable

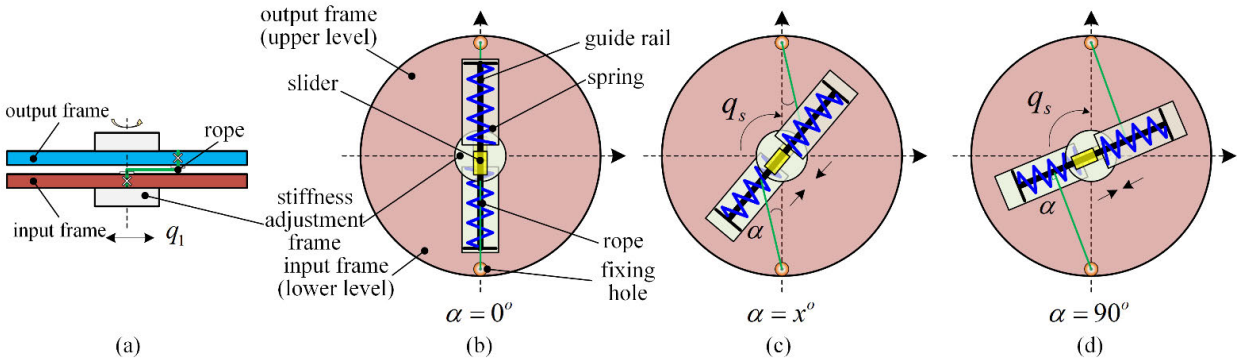

FIGURE 1. Schematic diagram of the proposed variable stiffness mechanism: (a) Description of the positional relationship between the output frame and input frame; (b) Minimum stiffness state; (c) Operating state of the variable stiffness mechanism; (d) Maximum stiffness state.

stiffness mechanism is designed and analyzed in Section II. Based on this, in Section III, a new VSA is designed. The performance analysis and simulations to evaluate the proposed VSA are presented in Sections IV. Finally, the conclusion is presented in Section V.

II. VARIABLE STIFFNESS MECHANISM DESIGN AND ANALYSIS

A. ABBREVIATIONS AND ACRONYMS

Fig. 1 shows the stiffness adjustment principle of the proposed design. For the convenience of observation, the output frame in Fig. 1 (b)-(d) has been temporarily hidden. As shown in Fig. 1 (a) and (b), a stiffness adjustment frame is coaxially installed in the middle of the input frame and output frame. On this stiffness adjustment frame, a pair of guide rail sliders are symmetrically arranged in space. The sliders are installed on the stiffness adjustment frame, and the guide rail can slide on the sliders within a certain range. One end of the guide rail is equipped with a compression spring, and the other end is connected to a rope. The rope is fixedly connected to the edge fixing holes of the input or output frame through the edge fixing hole of the input frame or output frame.

If the output frame does not rotate relative to the input frame, the spring and rope states are shown in Fig. 1 (a), where the angle between the rope and the extension line of the guide rail is defined as α. As shown in Fig. 1 (b), rotate the stiffness adjustment frame by a certain angle q_s relative to the input frame, because the rope length is constant, then one end of the guide rail compresses the spring and extends a certain length along the slider, while α also increases. As shown in Fig. 1 (d), as q_s increases, α also continues to increase to 90°, at which point the rope and guide rail are perpendicular. Overall, during the process of α changing from 0 to 90°, the output stiffness of the variable stiffness mechanism (VSM) also varies from the minimum value to approximately infinite. Therefore, by controlling the angle q_s of the stiffness adjustment frame relative to the input frame, the output stiffness of the VSM can be continuously adjusted over a large range.

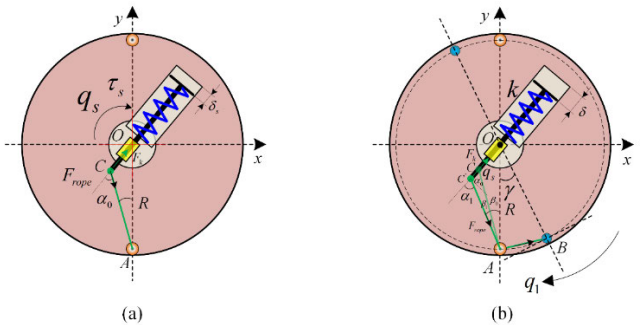

FIGURE 2. Schematic diagram of force analysis: (a) Force analysis of the stiffness adjustment process when there is no relative deflection between the input and output frames; (b) Force analysis when there is relative deflection γ between input and output frames.

B. STIFFNESS MODELING OF THE VSM

Due to the symmetry of the structure, for the convenience of analysis, as shown in Fig. 2 (a), only the force situation of the unilateral spring during the stiffness adjustment process is analyzed, where there is no relative deflection between the input and output frames. Assuming that the elastic expansion and contraction rate of the rope is negligible. The spring is rotated by a certain angle q_s relative to the input frame, and the guide rail extends a certain length δ_s relative to the slider. The spring will be compressed during this process, thus generating resistance torque on the stiffness adjustment frame. Therefore, the required stiffness adjustment torque τ_s can be calculated by

$$\tau_s = nF_{rope}\overline{CO}\sin\alpha_0 \tag{1}$$

where n is the number of springs in the VSM, F_{rope} is the tension of the rope, α_0 is the angle between the guide rail and the rope without deflection.

According to Hooke's law, the force F_k exerted by the spring on the guide rail is

$$F_k = k(\delta_0 + \delta_s) \tag{2}$$

where k and δ_0 are the stiffness constant and the pre-compression length of the spring, respectively.

According to the force balance relationship, there are

$$F_k = F_{rope} \cos \alpha_0. \tag{3}$$

Thus, the required stiffness adjustment torque τ_s can be rewritten as

$$\tau_s = nk(\delta_0 + \delta_s)\overline{CO} \tan \alpha_0. \tag{4}$$

According to the sine theorem of a triangle, the relationship between α_0 and q_s can be derived as

$$\alpha_0 = \arcsin\left(\frac{R \sin q_s}{r_0}\right) \tag{5}$$

where R and r_0 are the distance of $\overline{OA}$ and the length of the rope, respectively.

Based on the above analysis, the adjustment range of q_s to change the output stiffness of the joint can be calculated by

$$0^o \le q_s \le \arcsin\left(r_0/R\right). \tag{6}$$

Further based on the triangle sine theorem, it can be obtained that

$$\delta_s = \frac{R - r_0 \cos(\alpha_0 - q_s)}{\cos q_s} - R + r_0. \tag{7}$$

Obviously, $\alpha_0 = 0^o$ when $q_s = 0^o$, and if there is no deflection ($\gamma = 0^o$), $\delta_s = 0$ which means no load is applied on the joint actuator.

However, as shown in Fig. 2 (b), α_0 will increase to α_1 with the actuator deflection. Then, the compression of the spring will become

$$\delta = \delta_s + \delta_e \tag{8}$$

where δ_e is the additional spring compression caused by elastic deflection (external load force).

The chord length $\overline{AB}$ of the elastic deflection section between the input and output frames can be calculated by

$$\overline{AB} = 2R \sin \frac{\gamma}{2} \tag{9}$$

where $\gamma = \angle AOB = q_2 - q_1$ is the deflection angle of the actuator, q_1 and q_2 are the angles of the input frame and the output frame, respectively.

Because the total length of the rope r_0 is a constant, after ignoring the stretching of the rope, it can be obtained that

$$\overline{C'A} = \overline{CA}_0 - \overline{AB} = r_0 - 2R \sin \frac{\gamma}{2}. \tag{10}$$

Combining the sine theorem of a triangle again, the relationship between α_1 and q_s can be defined as

$$\alpha_1 = \arcsin\left(\frac{R \sin q_s}{\overline{C'A}}\right) = \arcsin\left(\frac{R \sin q_s}{r_0 - 2R \sin \frac{\gamma}{2}}\right). \tag{11}$$

Referring to Eq. (2), the force exerted by the spring on the guide rail can be recalculated by

$$F_k = k(\delta_0 + \delta) = k(\delta_0 + \delta_s + \delta_e). \tag{12}$$

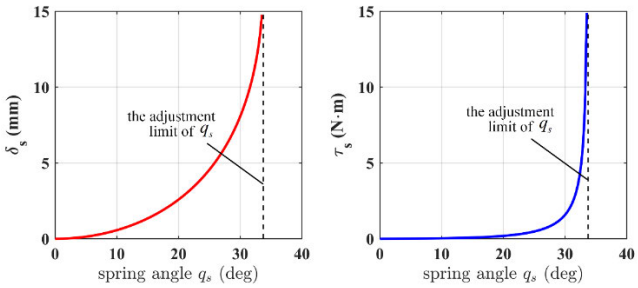

FIGURE 3. Theoretical analysis of independent motion of the VSM: (a) Change in spring compression; (b) The required stiffness adjustment torque.

Referring to Eq. (3), and ignoring the frictional force when the rope passes through hole A, the elastic driving torque τ_e of the tension on the rope on the output frame can be calculated by

$$\tau_e = nF_{rope}R \cos \frac{\gamma}{2} = \frac{nkR(\delta_0 + \delta_s + \delta_e)}{\cos \alpha_1} \cos \frac{\gamma}{2}. \tag{13}$$

And δ_e is caused by γ, which can be defined as

$$\overline{C'O} = \overline{CO}_0 + \delta_s + \delta_e. \tag{14}$$

Referring to Eqs. (9) and (13), and the geometric relationship, it can be obtained that

$$\delta_s + \delta_e = \frac{R - \left(r_0 - 2R \sin \frac{\gamma}{2}\right) \cos(\alpha_1 - q_s)}{\cos q_s} - \overline{CO}_0. \tag{15}$$

In fact, the length of the $\overline{AB}$ mapped to the axial elongation of the guide rail can be defined as

$$\begin{aligned} \delta_e &= \overline{CA}_0 \cos \alpha_0 - \overline{C'A} \cos \alpha_1 \\ &= r_0 \cos \alpha_0 - (r_0 - 2R \sin \frac{\gamma}{2}) \cos \alpha_1. \end{aligned} \tag{16}$$

Usually, the output stiffness of the actuator can be calculated by

$$K_a(q_s, \gamma) = \frac{\partial \tau_e}{\partial \gamma}. \tag{17}$$

C. ANALYSIS OF THE PROPOSED VSM

In order to determine the key design parameters of the VSA, it is necessary to analyze its characteristics to determine design constraints. Referring to Eq. (7), when adjusting the spring angle q_s independently, the spring compression can vary nonlinearly, as shown in Fig. 3(a). Similarly, as shown in Fig. 3(b), the resistance torque of the VSM transmission chain increases sharply after the spring angle exceeds 30°, which means that the stiffness adjustment motor drive requires a larger peak torque or reduction ratio.

Referring to Eq. (17), the output stiffness change trend of the VSA without deflection shown in Fig. 4 is similar to that of τ_s. Although a high transmission ratio of the stiffness adjustment drive chain may lead to a decrease in the response speed of the stiffness adjustment, the adjustment limit range

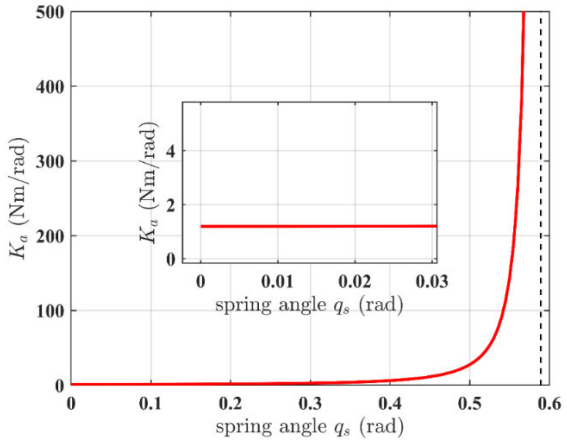

FIGURE 4. Stiffness of the SVSA in different spring angle q_s in zero deflection angle.

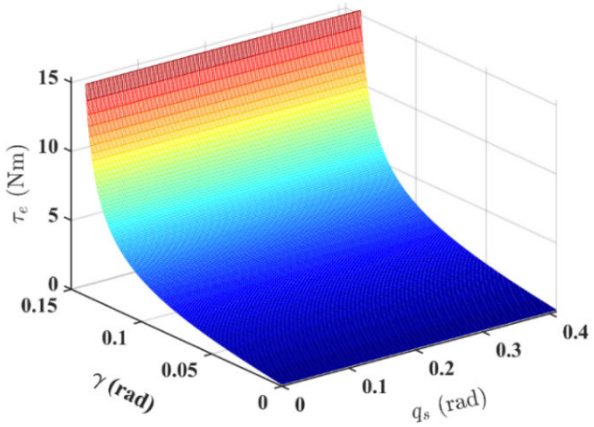

FIGURE 6. The elastic driving torque of the actuator under the coupling effect of the spring angle and deflection angle.

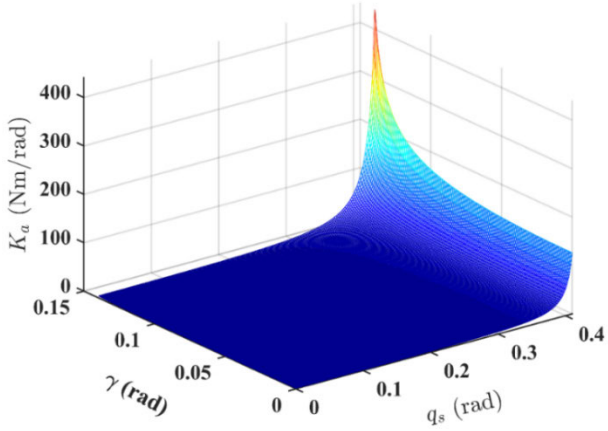

FIGURE 5. Theoretical stiffness under the coupling effect of the spring angle and deflection angle.

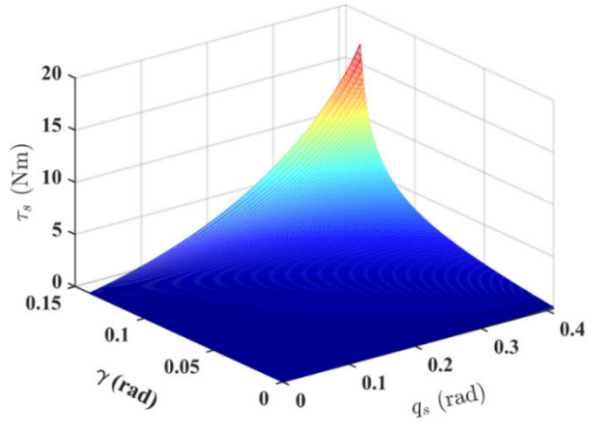

FIGURE 7. Resistance torque of the VSM under the coupling effect of the spring and deflection angles.

of q_s is approximately within 35 ° (refer to Fig. 3), and the stiffness change is sharp when q_s is greater than 30 °, making rapid stiffness adjustment possible. In addition, as an adjustable passive compliant robot joint, from an application perspective, the resolution of adjustment in high stiffness areas ($q_s \geq 35^0$) has sharply decreased, and its regulation has almost no practical significance.

Referring to Eq. (17), when the output frame of the VSA is subjected to a load, it will deflect, and the output stiffness of the actuator will be additionally affected by the coupling effect of the deflection, as shown in Fig. 5. From a macro perspective, in most of the coupling regulation regions of q_s and γ, the linearity of stiffness changes is smooth, which is conducive to achieving accurate and rapid stiffness adjustment response. Therefore, the design and selection of the adjustable stiffness drive chain do not need to overly emphasize the global control response speed.

Referring to Eq. (13), when the actuator deflects, the ropes are pulled by the input and output frames, and the elastic torque generated can be used to drive the load. The dynamic characteristics of τ_e are shown in Fig. 6, where q_s has a minimal impact on τ_e. This means that the online stiffness adjustment has a slight impact on stable elastic torque output, which is beneficial for improving the independence of the stiffness adjustment and the output position q_2. In addition, the transmission design of the main drive motor can refer to the peak torque and change rate along γ in Fig. 6.

Under the coupling effect of the elastic deflection and spring angle, the resistance torque suffered by the VSM defined in Eq. (4) can be rewritten as

$$\begin{aligned}\tau_s &= nF_{rope}\sin\alpha_1\overline{C'O} \\ &= \frac{nk(\delta_0+\delta_s+\delta_e)\sin\alpha_1}{\cos\alpha_1}(\overline{CO}_0+\delta_s+\delta_e). \end{aligned} \tag{18}$$

Under this working condition, the change in resistance torque reflected on VSM is shown in Fig. 7. Obviously, the impact of changes in q_s on the required stiffness adjustment torque τ_s shows an approximate linear trend, but the impact of γ on it shows a significant nonlinearity. This indicates

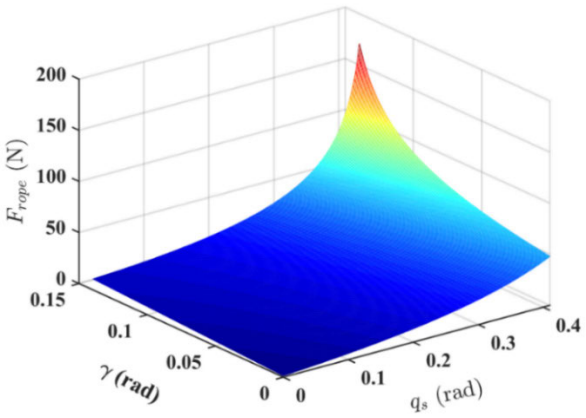

FIGURE 8. The tension of the rope under the coupling effect of the spring angle and deflection angle.

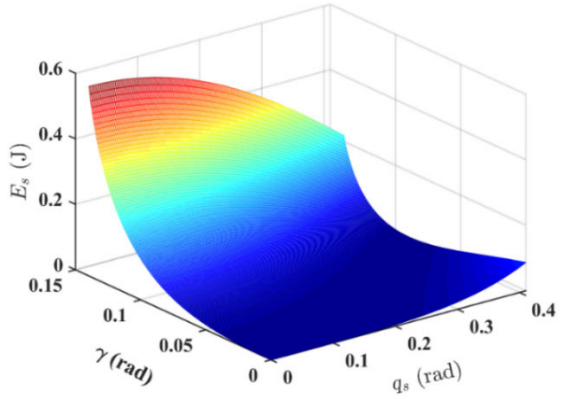

FIGURE 9. The elastic energy storage of the VSA under the coupling effect of the spring angle and deflection angle.

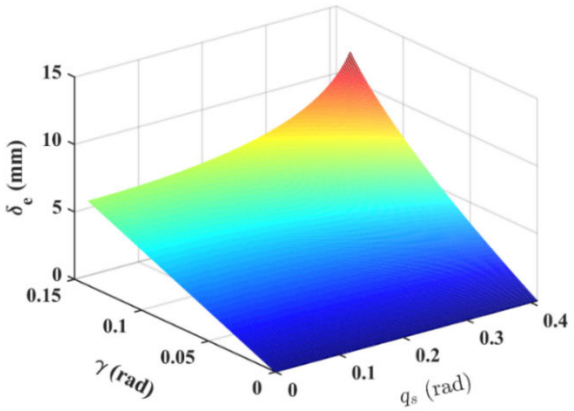

FIGURE 10. The change in spring compression of the VSM during the dynamic process of the VSA.

that changes in load will have a certain impact on the VSM. When designing the stiffness adjustment drive chain, the issue of stiffness maintenance should be considered (for example, worm gear and worm transmission mechanisms with self-locking effects can be adopted).

Referring to Eqs. (3) and (12), in addition, when designing the VSA, the ropes used need to meet a certain level of strength and toughness, so the tension change of the ropes under the coupling effect of load and stiffness adjustment should be considered. Fig. 8 shows that the tension change of the rope is relatively mild in most of the stiffness adjustment areas. Referring to the tension change of the rope in extreme cases ($q_s > 0.3rad, \gamma > 0.1rad$), it can provide a reliable basis for the selection of the ropes.

The elastic mechanism of a VSA can store energy and reuse this part of energy during periodic motion, achieving energy-saving motion control and shock absorption, achieving a safe physical interaction effect of buffering and vibration absorption [9]. In this design, the elastic energy storage E_s of the proposed VSA can be calculated by

$$E_s(q_s, \gamma) = \int_0^{\gamma} \tau_e d\gamma. \tag{19}$$

Fig. 9 shows that the change in E_s is mainly influenced by the deflection γ, but when there is no deflection, a small amount of elastic energy is still stored in the spring compression due to the change in preload (caused by q_s adjustment), which is a characteristic of VSA based on the principle of preload adjustment.

In order to ensure the reasonable design of the springs in the VSM, the selection of the spring should not only comprehensively consider its total length, stiffness constant, material, etc., but also consider the deformation situation after assembly under the coupling effect of the pre-compression, load, and the stiffness adjustment. Fig. 10 shows the change in spring compression of the VSM during the dynamic process of the VSA.

TABLE 1. Key design parameters of the proposed VSA.

Parameters	Value	Unit
Size of the actuator	107*239* ϕ 110	mm
Weight of the actuator (theoretical)	2.67	kg
Gear ratio of main drive chain	172	
Gear ratio of the VSM chain	160	
Nominal output torque	23	Nm
Nominal output speed	14.7	rpm
Output motion range (q_2)	360	°
Stiffness adjustment range (K_a)	2.7~∞	Nm/rad
Spring constant (k)	1.5	N/mm
Drive arm (R)	45	mm
Rope length (r_0)	25	mm
Spring pre-compression (δ_0)	3	mm

III. VARIABLE STIFFNESS ACTUATOR DESIGN

Based on the VSM described above, a VSA was designed, as shown in Figs. 6-9. The actuator consists of the following three parts, which will be explained from the outside to the inside of the VSA, and its key design parameters are shown in Table 1.

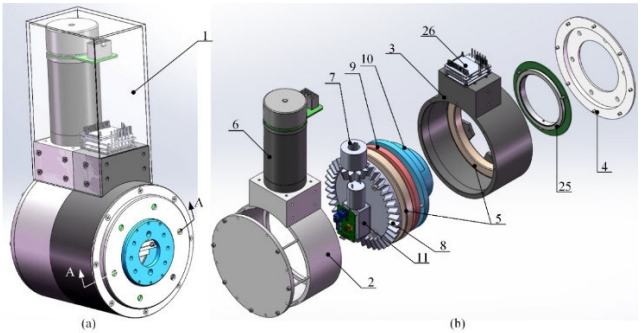

FIGURE 11. CAD model of the proposed VSA: (a) Overall isometric view; (b) Partial explosion view; 1-4: protective cases, 5-large bearings, 6-position motor, 7-8: bevel gears, 9-input frame, 10-output frame, 11-stiffness adjustment motor, 25-encoder.

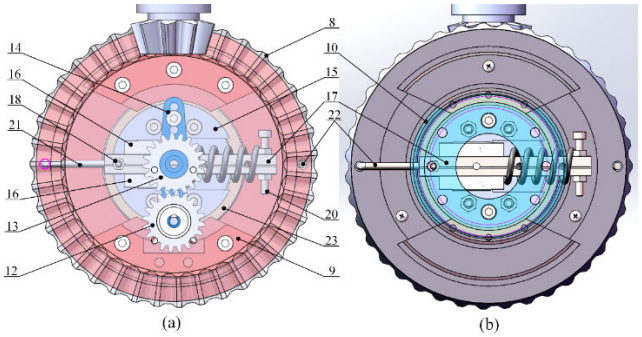

FIGURE 13. Schematic diagram of the main rotating module: (a) Backward view; (b) Forward view; 8-bevel gear, 12-driving gear, 13-driven gear, 14-transmission beam, 15-stiffness adjustment frames, 16-slider, 17-guide rail, 18-guide rail limit bolt, 20-spring limit bolt, 21-22: ropes, 23-small bearing.

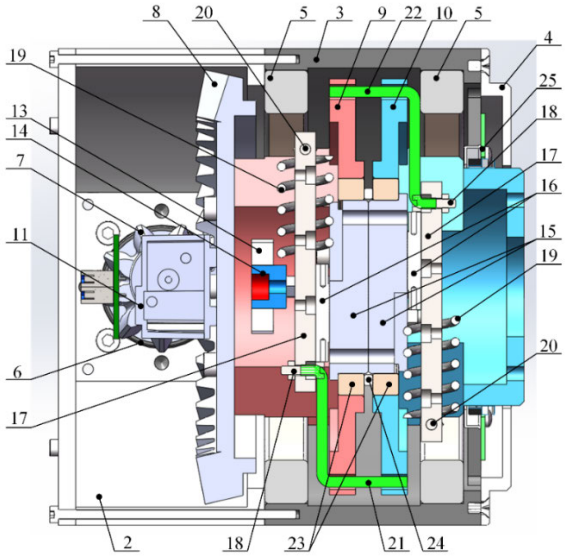

FIGURE 12. Sectional view along the A-A direction in Figure 11(a) : 13-driven gear, 14-transmission beam, 15-stiffness adjustment frames, 16-slider, 17-guide rail, 18-guide rail limit bolt, 19-spring, 20-spring limit bolt, 21-22: ropes, 23-small bearings, 24-ring, 25-encoder.

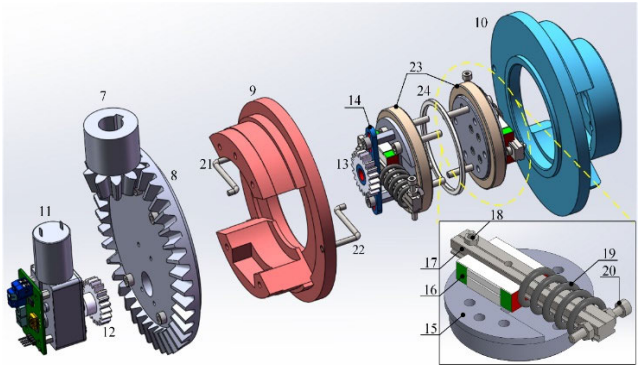

FIGURE 14. Explosion view of the main rotating module. 7-8: bevel gears, 9-input frame, 10-output frame, 11-stiffness adjustment motor, 12-driving gear, 13-driven gear, 14-transmission beam, 15-stiffness adjustment frames, 16-slider, 17-guide rail, 18-guide rail limit bolt, 19-spring, 20-spring limit bolt, 21-22: ropes, 23-small bearing, 24-ring, 25-encoder.

(1) Protective cases: As shown in Fig. 11, parts 1-4 form the protective bases of the whole VSA, which take into account the protection of internal moving components and the role of force transmission in robot applications. Among them, the end face of the part 2 can be used to connect the remaining links of a robot. Part 4 is used to protect the encoder (part 25). Part 2 is used to withstand all loads and weights.

(2) Main drive module: As shown in Fig. 11 and Fig. 12, parts 8-24 can be considered as a whole rotating relative to part 2 based on a pair of large bearings (part 5). The position motor (part 6) is mounted on the protective case (part 2). The main drive power from the position motor (part 6) is transmitted to the large bevel gear (part 8) installed at one end of the input frame (part 9) through a small bevel gear (part 7), and then to the output frame (part 10) through a pair of ropes (parts 21-22). The load can be connected to one end of the output frame (part 10). In addition, the inner ring of the encoder (part 25) is fixed on the output frame and the reading head is installed at the protective case (part 2) end, which can be used to obtain the position of the output frame. The position of the input frame can be calculated by the encoder and reduction ratio of the position motor.

(3) Stiffness adjustment mechanism: As shown in Figs. 11-14, the stiffness adjustment motor (part 11) with self-locking characteristics is installed on the large bevel gear (part 8). Then, a pair of small gears (part 12 shown in Figure 13 and part 13) are installed on the stiffness adjustment motor and transmission beam (part 14) which is fixed on a stiffness adjustment frame (part 15), respectively. As shown in Fig. 11 and Fig. 13, a pair of the stiffness adjustment frames (part 15) symmetrically installed at respective end faces with respect to the origin point in space. In order to provide adjustable stiffness characteristics for the ropes (parts 21-22) located between the input frame and output frame, a linear telescopic elastic module is installed on a stiffness adjustment frame (part 15) shown in Figs. 13-14, which consists of a slider (part 16), a guide rail (part 17), a guide rail limit bolt (part 18), a spring (part 19) and a spring limit bolt (part 20). The spring is installed coaxially with the guide rail, and its

two ends are respectively limited by the slider and the spring limit bolt. The slider is mounted on the one end of the stiffness adjustment frame and rotates together with it. The guide rail can move back and forth on the slider and is limited by the guide rail limit bolt and the spring.

As shown in Fig. 12 and Fig. 13, one end of a rope (part 21) is fixed at the position of the guide rail limit bolt (part 18), and the other end of this rope is fixed at the corresponding hole on the output frame (part 10) through the hole on the edge of the input frame (part 9). On the contrary, one end of the another rope (part 22) is fixed at the position of the guide rail limit bolt (part 18), and the other end of this rope is fixed at the corresponding hole on the input frame (part 9) through the hole on the edge of the output frame (part 10). Obviously, the drive power between the input and output frames is transmitted in series through the ropes (parts 21-22). When there is a deflection between the input frame and the output frame, the ropes are pulled, which in turn pull the guide rails to move along the sliders and ultimately compress the springs. Therefore, by adjusting the angle of the stiffness adjustment frames (part 15) relative to the input and output frames (parts 9 and 10), the angle between the spring (part 19) axis (or the guide rail (part 17)) and the rope (part 21 or 22) can be changed, and the pre tightening force of the rope (part 21 or 22) can be adjusted, and the output stiffness of the actuator can be adjusted ultimately. The spring angle relative to the input frame can be calculated by combining the encoder of the stiffness adjustment motor with the reduction ratio.

As shown in Figs. 12-14, a pair of elastic modules (parts 15-20) are supported and installed in the input and output frames respectively through a pair of small bearings (part 23), which can be can be driven by the stiffness adjustment motor (part 11) and rotated relative to the input frame or the output frame. To avoid motion interference, a ring (part 24) is installed between the two elastic modules. Referring to Eqs. (6), (16), and Fig. 1, the VSA can achieve a larger stiffness adjustment bandwidth within a small rotation range, which is beneficial for improving the stiffness adjustment response speed. In addition, in order to avoid jamming between the input frame and the output frame when the ropes are completely relaxed, the length of the rope components should be controlled during assembly, so that the spring produces a certain amount of pre compression.

IV. PERFORMANCE SIMULATION OF THE PROPOSED VSA

A. DYNAMIC MODEL OF THE VSA

As mentioned above, referring to Fig. 14, the proposed VSA is essentially a series elastic driving configuration. The VSM is supported on the input and output frames, but its relative position is mainly constrained by the input frame. Therefore, the dynamic model of the entire VSA is shown in Fig. 15.

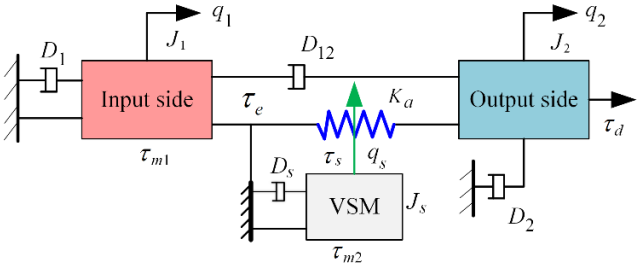

FIGURE 15. Schematic diagram of the kinetic model of the proposed VSA.

TABLE 2. Key dynamic parameters of the proposed VSA.

Parameters	Value	Unit
Output side inertia (J_2)	$2.78*10^{-5}$	kgm^2
Input side inertia (J_1)	$1.43*10^{-4}$	kgm^2
Inertia of the VSM (J_s)	$4.78*10^{-6}$	kgm^2
D_2	$1.2*10^{-3}$	Nms/rad
D_1	$2.9*10^{-3}$	Nms/rad
D_s	$4.8*10^{-3}$	Nms/rad
D_{12}	$1.2*10^{-3}$	Nms/rad
Load mass	2	kg
Link length (L)	300	mm

As shown in Fig. 15, the actuator dynamics can be modeled by [24]

$$\begin{aligned} J_2\ddot{q}_2 + D_2\dot{q}_2 + G(q_2) + \tau_d &= \tau_e \\ J_1\ddot{q}_1 + D_1\dot{q}_1 + \tau_e &= \tau_{m1} \\ J_s\ddot{q}_s + D_s\dot{q}_s + \tau_s &= \tau_{m2} \end{aligned} \tag{20}$$

where q_1, q_2 and q_s are the angular displacements of the input frame, the output frame, and the VSM, respectively. J_1, J_2 and J_s are the reflected inertias of the input frame, the output frame, and the VSM, respectively, D_1, D_2 and D_s are the equivalent damping coefficients for the input frame, the output frame, and the VSM, respectively, $G(q_2)$ is the gravitational torque acting on the output frame, τ_d is a lumped disturbance torque that includes the load torque and model uncertainties such as hysteresis, friction, and internal damping, τ_s is the resistant torque on the VSM, which represents the influence of the deflection γ, τ_{m1} and τ_{m2} are the equivalent driving torque acting on each motor, and τ_e is the spring elastic torque given by

$$\tau_e = K_a(q_s, \gamma)\gamma(q_1, q_2) \tag{21}$$

In order to conduct dynamic performance simulation analysis on the VSA, its main dynamic parameters are shown in Table 2.

B. CONTROLLER DESIGN

To verify the basic motion performance of the proposed VSA, PD controllers were designed for the main drive chain (with

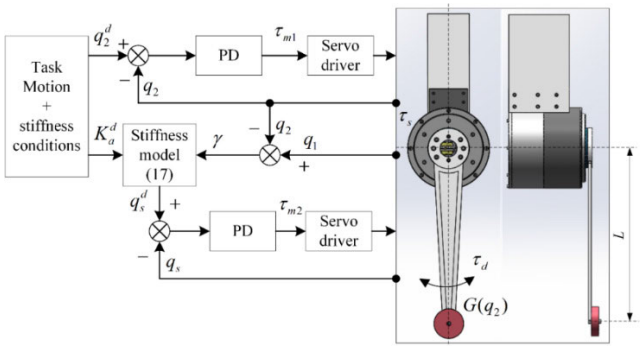

FIGURE 16. Control block diagram and joint simulation settings.

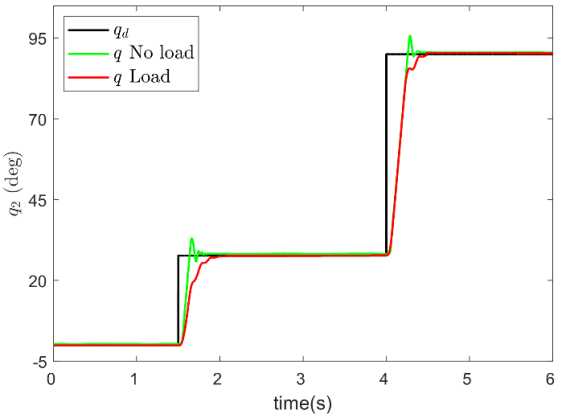

FIGURE 17. Step response for the main position control.

gravity compensation) and the VSM drive chain, respectively, which is shown in Fig. 16. The output frame of the VSA is connected with a load and set as a whole to the horizontal state of the joint axis. The position information on the input and output frames is used to calculate the deflection angle. Then, based on the stiffness model defined by Eq. (17), the required spring angle can be calculated.

C. SIMULATION RESULTS

The step response of the output frame position of the main drive module under a moderate stiffness level is shown in Fig. 17. In the small travel step response, the tracking response is relatively fast at no-load, and the steady-state time is significantly longer with the increase of load. In the step response of larger travel, due to the acceleration, the steady-state time under load condition decreases, which also shows the effectiveness of gravity compensation mention above.

For a VSA, its stiffness response speed is a very important indicator. Therefore, for the proposed VSA, the spring angle step response of small stroke and large stroke is carried out, as shown in Fig. 18 (a), and the corresponding actuator output stiffness based on Eq. (17) is shown in Fig. 18 (b). It can be seen that there is not much difference in the response speed of the VSM under no-load and load conditions, which once

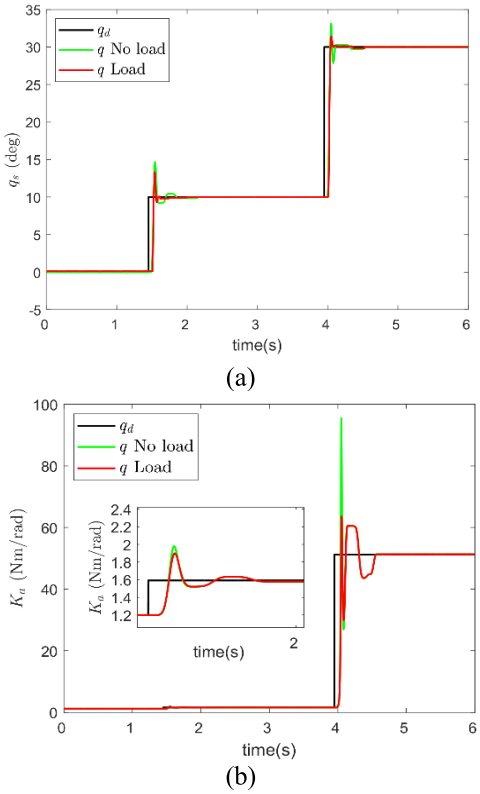

FIGURE 18. Step response for the main position control: (a) Spring angle; (b) Corresponding stiffness.

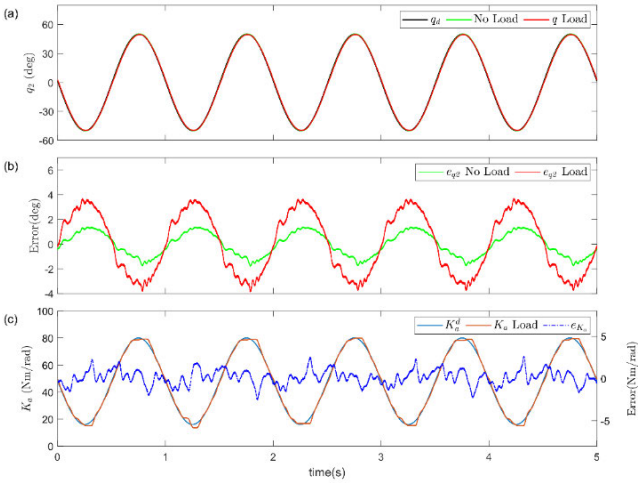

FIGURE 19. Trajectory tracking performance: (a) Output position; (b) Position tracking error; (c) Stiffness tracking results under the load condition.

again verifies the results shown in Fig. 5 (the deflection angle γ has a slight impact on K_a).

Fig. 19 shows the position and stiffness synchronization tracking control effect of the VSA. The main drive output frame tracks a sinusoidal trajectory signal with a frequency of 1 Hz and an amplitude of 50 degrees under no-load and load conditions. The output position tracking performance and tracking error are shown in Fig. 19 (a) and (b), respectively.

Obviously, the load has a certain deteriorating effect on the tracking performance. In addition, to verify the performance of synchronous variable stiffness, under load conditions, the VSM is also tracking a sinusoidal signal with a frequency of 1 Hz and an amplitude of 35 Nm/rad, with a tracking error of approximately 4.7 Nm/rad, as shown in Fig. 19(c). Because the synchronous tracking effect of the stiffness under no-load conditions is relatively ideal and has little reference significance, it has not been shown yet.

V. CONCLUSION

A new type of VSA that can simultaneously adjust the position and output stiffness independently is developed in this paper. The VSM based on the spring angle adjustment and rope pre-tension adjustment makes smooth and fast stiffness adjustment possible. The relative angle between the rope and the spring axis allows the actuator to have a large stiffness adjustment range. The entire VSA has modular design features. The model accuracy and the design performance are demonstrated by regulation and tracking simulations. Our next research direction is to manufacture a prototype of the proposed VSA for performance testing and apply it to a multi degree of freedom flexible robot. More advanced or personalized control algorithms will be designed for the VSA control.

REFERENCES

[1] N. Hogan, "Contact and physical interaction," *Annu. Rev. Control, Robot. Auton. Syst.*, vol. 5, no. 1, pp. 179–203, May 2022.
[2] A. Calanca and P. Fiorini, "On the role of compliance in force control," in *Intelligent Autonomous Systems* (Advances in Intelligent Systems and Computing), vol. 302, E. Menegatti, N. Michael, K. Berns, and H. Yamaguchi, Eds. Cham, Switzerland: Springer, 2016, pp. 1243–1255.
[3] A. Calanca, R. Muradore, and P. Fiorini, "A review of algorithms for compliant control of stiff and fixed-compliance robots," *IEEE/ASME Trans. Mechatronics*, vol. 21, no. 2, pp. 613–624, Apr. 2016.
[4] F. Petit, A. Dietrich, and A. Albu-Schäffer, "Generalizing torque control concepts: Using well-established torque control methods on variable stiffness robots," *IEEE Robot. Autom. Mag.*, vol. 22, no. 4, pp. 37–51, Dec. 2015.
[5] S. Haddadin, A. De Luca, and A. Albu-Schäffer, "Robot collisions: A survey on detection, isolation, and identification," *IEEE Trans. Robot.*, vol. 33, no. 6, pp. 1292–1312, Dec. 2017.
[6] J. de Gea Fernández, B. Yu, V. Bargsten, M. Zipper, and H. Sprengel, "Design, modelling and control of novel series-elastic actuators for industrial robots," *Actuators*, vol. 9, no. 1, p. 6, Jan. 2020.
[7] L. Sun, M. Li, M. Wang, W. Yin, N. Sun, and J. Liu, "Continuous finite-time output torque control approach for series elastic actuator," *Mech. Syst. Signal Process.*, vol. 139, May 2020, Art. no. 105853.
[8] M. Zhang, P. Ma, F. Sun, X. Sun, F. Xu, J. Jin, and L. Fang, "Dynamic modeling and control of antagonistic variable stiffness joint actuator," *Actuators*, vol. 10, no. 6, p. 116, May 2021.
[9] S. Wolf, G. Grioli, O. Eiberger, W. Friedl, M. Grebenstein, H. Höppner, E. Burdet, D. G. Caldwell, R. Carloni, M. G. Catalano, and D. Lefeber, "Dynamic modeling and control of antagonistic variable stiffness joint actuator," *IEEE/ASME Trans. Mechatronics*, vol. 21, no. 5, pp. 2418–2430, Nov. 2015.
[10] M. Harder, M. Keppler, X. Meng, C. Ott, H. Höppner, and A. Dietrich, "Simultaneous motion tracking and joint stiffness control of bidirectional antagonistic variable-stiffness actuators," *IEEE Robot. Autom. Lett.*, vol. 7, no. 3, pp. 6614–6621, Jul. 2022.
[11] P. Bilancia, G. Berselli, and G. Palli, "Virtual and physical prototyping of a beam-based variable stiffness actuator for safe human-machine interaction," in *Proc. IEEE/ASME Int. Conf. Adv. Intelli. Mechatronics (AIM)*, Sapporo, Japan, Oct. 2020, Art. no. 101886.
[12] X. Xiong, X. Sun, W. Chen, Y. Zhi, and X. Fang, "Design of a variable stiffness actuator based on variable radius mechanisms," in *Proc. IEEE/ASME Int. Conf. Adv. Intell. Mechatronics (AIM)*, Jul. 2022, pp. 1567–1572.
[13] A. Jafari, H. Q. Vu, and F. Iida, "Determinants for stiffness adjustment mechanisms," *J. Intell. Robotic Syst.*, vol. 82, nos. 3–4, pp. 435–454, Jun. 2016.
[14] S. Wolf and G. Hirzinger, "A new variable stiffness design: Matching requirements of the next robot generation," in *Proc. IEEE Int. Conf. Robot. Autom.*, May 2008, pp. 1741–1746.
[15] S. Wolf and J.-E. Feenders, "Modeling and benchmarking energy efficiency of variable stiffness actuators on the example of the DLR FSJ," in *Proc. IEEE/RSJ Int. Conf. Intell. Robots Syst. (IROS)*, Oct. 2016, pp. 529–536.
[16] R. Van Ham, B. Vanderborght, M. Van Damme, B. Verrelst, and D. Lefeber, "MACCEPA, the mechanically adjustable compliance and controllable equilibrium position actuator: Design and implementation in a biped robot," *Robot. Auto. Syst.*, vol. 55, no. 10, pp. 761–768, Oct. 2007.
[17] S. Heins, L. Flynn, J. Geeroms, D. Lefeber, and R. Ronsse, "Torque control of an active elastic transfemoral prosthesis via quasi-static modelling," *Robot. Auto. Syst.*, vol. 107, pp. 100–115, Sep. 2018.
[18] Z. Li, S. Bai, O. Madsen, W. Chen, and J. Zhang, "Design, modeling and testing of a compact variable stiffness mechanism for exoskeletons," *Mechanism Mach. Theory*, vol. 151, Sep. 2020, Art. no. 103905.
[19] Y. Liu, S. Cui, and Y. Sun, "Mechanical design and analysis of a novel variable stiffness actuator with symmetrical pivot adjustment," *Frontiers Mech. Eng.*, vol. 16, no. 4, pp. 711–725, Dec. 2021.
[20] A. Jafari, N. G. Tsagarakis, and D. G. Caldwell, "A novel intrinsically energy efficient actuator with adjustable stiffness (AwAS)," *IEEE/ASME Trans. Mechatronics*, vol. 18, no. 1, pp. 355–365, Feb. 2013.
[21] A. Jafari, N. G. Tsagarakis, I. Sardellitti, and D. G. Caldwell, "A new actuator with adjustable stiffness based on a variable ratio lever mechanism," *IEEE/ASME Trans. Mechatronics*, vol. 19, no. 1, pp. 55–63, Feb. 2014.
[22] N. G. Tsagarakis, I. Sardellitti, and D. G. Caldwell, "A new variable stiffness actuator (CompAct-VSA): Design and modelling," in *Proc. IEEE/RSJ Int. Conf. Intell. Robots Syst.*, Sep. 2011, pp. 378–383.
[23] J. Sun, Z. Guo, D. Sun, S. He, and X. Xiao, "Design, modeling and control of a novel compact, energy-efficient, and rotational serial variable stiffness actuator (SVSA-II)," *Mechanism Mach. Theory*, vol. 130, pp. 123–136, Dec. 2018.
[24] D. Yang, H. Jin, Z. Liu, J. Fan, Y. Zhu, H. Zhang, and H. Dong, "Design and modeling of a torsion spring-based actuator (TSA) with valid straight-arm length adjustable for stiffness regulation," in *Proc. IEEE Int. Conf. Mechatronics Autom.*, Aug. 2016, pp. 2381–2386.
[25] S. S. Groothuis, G. Rusticelli, A. Zucchelli, S. Stramigioli, and R. Carloni, "The variable stiffness actuator vsaUT-II: Mechanical design, modeling, and identification," *IEEE/ASME Trans. Mechatronics*, vol. 19, no. 2, pp. 589–597, Apr. 2014.
[26] F. Frioli, "Variable stiffness actuators: The user's point of view," *Int. J. Robot. Res.*, vol. 34, no. 6, pp. 727–743, Mar. 2015.
[27] Z. Liu, H. Jin, H. Zhang, Y. Liu, Y. Long, X. Liu, and J. Zhao, "A variable stiffness actuator based on second-order lever mechanism and its manipulator integration," in *Proc. IEEE Int. Conf. Robot. Autom. (ICRA)*, May 2021, pp. 6999–7005.
[28] R. Ham, T. Sugar, B. Vanderborght, K. Hollander, and D. Lefeber, "Compliant actuator designs," *IEEE Robot. Autom. Mag.*, vol. 16, no. 3, pp. 81–94, Sep. 2009.
[29] L. Liu, B. J. E. Misgeld, A. Pomprapa, and S. Leonhardt, "A testable robust stability framework for the variable impedance control of 1-DOF exoskeleton with variable stiffness actuator," *IEEE Trans. Control Syst. Technol.*, vol. 29, no. 6, pp. 2728–2737, Nov. 2021.
[30] S. Yang, P. Chen, D. Wang, Y. Yu, and Y. Liu, "Design and analysis of a 2-DOF actuator with variable stiffness based on leaf springs," *J. Bionic Eng.*, vol. 19, no. 5, pp. 1392–1404, Sep. 2022.
[31] Y. Xu, K. Guo, J. Li, and Y. Li, "A novel rotational actuator with variable stiffness using S-shaped springs," *IEEE/ASME Trans. Mechatronics*, vol. 26, no. 4, pp. 2249–2260, Aug. 2021.
[32] Y. Xu, K. Guo, J. Sun, and J. Li, "Design, modeling and control of a reconfigurable variable stiffness actuator," *Mech. Syst. Signal Process.*, vol. 160, Nov. 2021, Art. no. 107883.
[33] T. Morrison, C. Li, X. Pei, and H.-J. Su, "A novel rotating beam link for variable stiffness robotic arms," in *Proc. Int. Conf. Robot. Autom. (ICRA)*, May 2019, pp. 9387–9393.

[34] J. Xiong, Y. Sun, J. Zheng, D. Dong, and L. Bai, "Design and experiment of a SMA-based continuous-stiffness-adjustment torsional elastic component for variable stiffness actuators," *Smart Mater. Struct.*, vol. 30, no. 10, Sep. 2021, Art. no. 105021.
[35] M. D. Christie, S. Sun, L. Deng, H. Du, S. W. Zhang, and W. H. Li, "Real-time adaptive leg-stiffness for roll compensation via magnetorheological control in a legged robot," *Smart Mater. Struct.*, vol. 31, no. 4, Feb. 2022, Art. no. 045003.
[36] Y. Xu, K. Guo, J. Sun, and J. Li, "Design and analysis of a linear digital variable stiffness actuator," *IEEE Access*, vol. 9, pp. 13992–14004, 2021.

YOULEI ZHAO received the master's degree in industrial engineering from Shandong University. He is currently pursuing the Ph.D. degree in industrial engineering with UCSI University. He is a Senior Researcher with the Shandong IoT Association. His current research interests include component design, the Internet of Things, and human–machine interaction control in-process production.

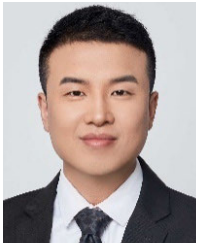

JUNQIANG LIU received the master's degree in mechanical engineering from Shandong University. He is currently a Product Design Engineer with Inspur Electronic Information Industry Company Ltd., where he is focusing on the Internet of Things, manufacturing design, and human–machine interaction control in-process production.

LI LI received the master's degree from the School of Computer Science and Technology, Shandong University of Finance and Economics. She is currently a Research Associate with the Jinan Radio Monitoring Station, where she is focusing on servo motion control of pan tilt, the Internet of Things, signal processing, and flexible drive design.

YAPENG XU received the Ph.D. degree in mechanical engineering from Shandong University, Jinan, China, in 2021. He is currently a Lecturer with the School of Mechanical and Electrical Engineering, Zhengzhou University of Light Industry, Zhengzhou, China. His current research interests include variable stiffness actuator design, modeling, motion control, and physical interaction between humans and robots.